Integrated Modular Motor Drives Based on Multiphase Axial-flux PM Machines with Fractional-slot Concentrated Windings

Peng Han, *Senior Member, IEEE*, Greg Heins*, *Member, IEEE*, Yibin Zhang, *Student Member, IEEE*, and Dan M. Ionel, *Fellow, IEEE*
SPARK Laboratory, ECE Dept., University of Kentucky, Lexington, KY, USA
* Regal Beloit Corporation, Australia, Rowville, VIC 3178, Australia

peng.han@ieee.org, greg.heins@regalbeloit.com, yibin.zhang@uky.edu, dan.ionel@ieee.org

***Abstract*—The integrated motor drive (IMD) concept with possible modularization has attracted much attention in a broad spectrum of applications ranging from low-power general-purpose industrial drives to high-power electric propulsion. This paper presents the feasibility study and performance evaluation of using common axial-flux permanent-magnet (AFPM) machines with fractional-slot concentrated windings in IMDs, with the same diameter and a minimum increase in its axial length. Different winding configurations are compared in terms of the torque/power capability and fault tolerance without changing the winding current rating. The possibility of further torque improvement is discussed from the perspective of making full use of the air-gap field harmonics produced by PMs. An AFPM machine available in the lab has been dissembled and used to build the proof-of-concept design, to show the feasibility of the proposed design and benefits of the IMD.**

***Index Terms*—Axial-flux PM machine, motor drive, fractional-slot concentrated winding**

I. Introduction

Integrated motor drives (IMDs) effectively reduce the overall mass and volume of motor drive systems by eliminating the drive enclosure and embedding the drive electronics directly inside the machine housing. With this integration, the cooling system can be shared by the motor and drive unit, and the power cables between machines and drives can be significantly shortened or even eliminated completely [1], [2]. To facilitate the manufacturing and improve the fault tolerance, IMDs tend to have modularized machines and inverters, and increased number of phases, such as designs presented in [3]–[5].

This paper takes a common 12-slot 10-pole (12s10p) axial-flux permanent machine (AFPM) machine as an example to explore the possiblities of achieving high-performance IMDs using electric machines with fractional-slot concentrated windings instead of the conventionally used distributed windings. The machine itself can be either aixal-flux or radial-flux, depending on the applications.

The studied 12s10p motor has three possible winding configurations, as illustrated in Fig. 1. It can be see that, either configured to have 2 phase, 3 phases or 6 phases, the two coils that are 180 mechanical degrees apart from each other belong to the same phase, which forms an independent phase winding supplied by a full H-bridge when connected in series or parallel, though the current flowing into these two coils are of the opposite directions. For the 2-phase and 3-phase configurations, the 12s10p motor has adjacent coils belonging to the same phase, which can be grouped together and supplied by a single phase leg to achieve the modularization of drive electronics. With these two features, all of the three winding configurations are suitable to be used in the IMD. These features are also very common in other motors using fractional-slot concentrated windings.

This paper is organized as follows. Section II presents the configuration of the proposed integrated modular motor drive (IMMD). Section III reports the comparison of different winding configurations in terms of the torque/power capability and fault tolerance, based on which the number of phase is selected. Section IV studies the potential of further torque improvement from the perspective of magnetomotive force (MMF) harmonics, followed by the proof-of-concept design and basic experimental testing results in Section V. Section VI concludes the full paper.

II. Proposed Integrated Modular Motor Drive

The proposed IMMD has m independent phases and each phase consists of two coil groups placed diametrically, as shown in Fig. 2, where m can be 2, 3, or 6 for the studied motor. There are $2m$ converter modules equally spaced in the circumferential direction. Each converter module is a single phase leg, which will be attached to one coil group. There are in total m H-bridges to supply the m phase, as shown in Fig. 3. In addition, in the case of high-power design, a double-sided heat sink is shared by the power converter and motor for more efficient cooling using liquids as the coolant. For low-power applications, two separate heat sinks may be used, one for the power converter and the other for the motor.

It should be noted that in the proposed IMMD, in order to maximize the degree of freedom of control, each single

Dr. Peng Han was with the SPARK Laboratory, ECE Department, University of Kentucky, Lexington, KY and is now with Ansys, Inc., San Jose, CA.

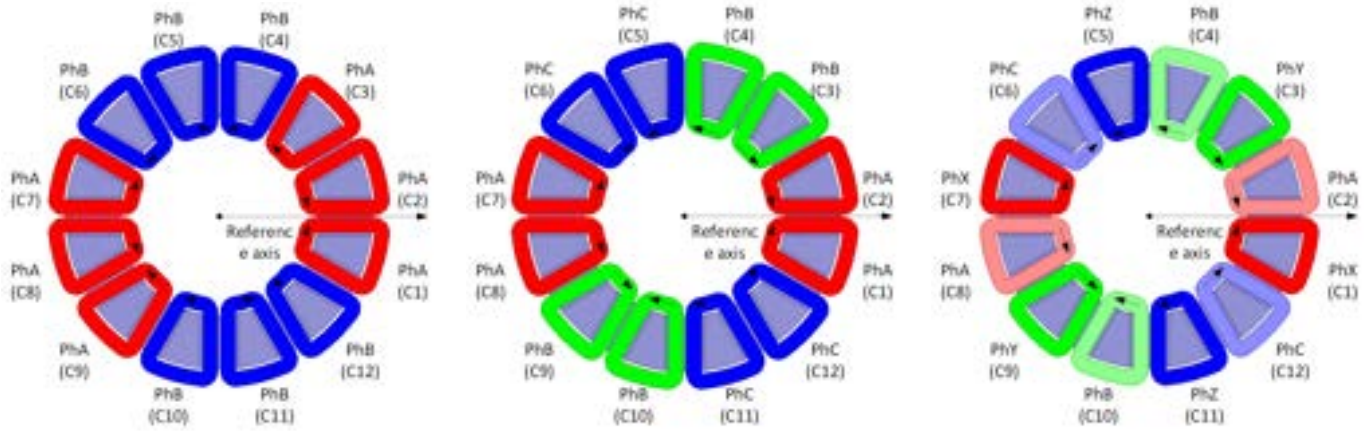

(a) (b) (c)

Fig. 1: Possible winding configurations, (a) 2-phase, (b) 3-phase, (c) 6-phase. Arrows denote the coil directions.

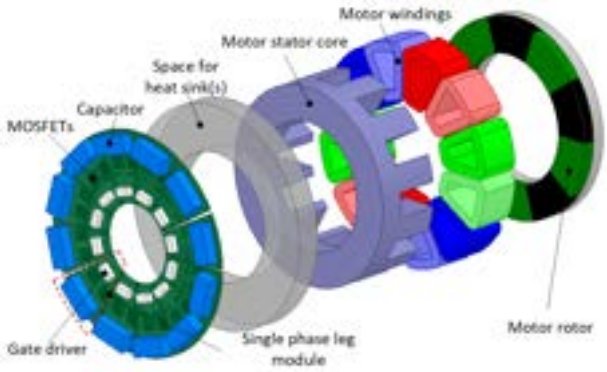

Fig. 2: Exploded view of the motor and drive assembly. Coils of the same color belong to the same phase. The case with m=6 is illustrated as an example.

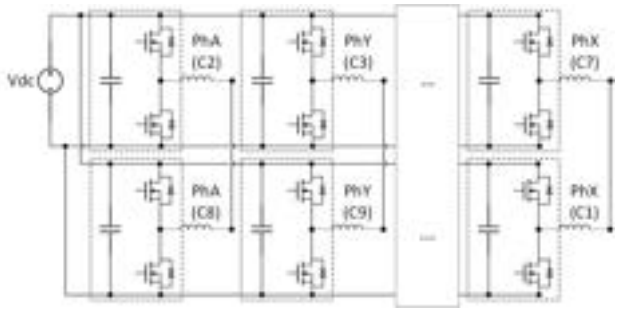

Fig. 3: Schematic diagram of the power converter and coil connection. The case with m=6 is illustrated as an example.

phase is supplied by an independent H-bridge and there is no neutral point. By introducing neutral points, the machine can still operate in the event of faults. This will reduce the switch count by half but the power rating of each switch will have to be increased accordingly.

III. Selection of Phase Number Based on Torque/Power Capability and Fault-tolerance

The 2-phase configuration has the unique feature of electromagnetically isolated phases leading to high fault tolerance as a generator, as shown in [6], and is suitable for low-cost motor drive with a single-phase input using as few as 6 switches. The 3-phase winding configuration shows an advantage by using the standard 3-phase converters.

In comparison with the 2-phase and 3-phase configurations, each individual phase of the 6-phase configuration can utilize the full dc bus voltage to achieve higher speed, or for the same speed rating, the voltage rating of switches can be reduced. With the same current rating, the 6-phase configuration will achieve the highest torque capability with pure sinusoidal current excitations considering the differences in winding factors (2-ph: 0.8797, 3-ph: 0.9330, and 6-ph: 0.9659).

The influence of the physical air-gap length on the open-circuit back-electromotive force (back-EMF) and torque for the three winding configurations is shown in Fig. 4a and Fig. 4b. The open-circuit back-EMF and torque constant at various air-gap lengths are shown considering the fact that it is usually difficult to accurately set up and measure the real air-gap length of an AFPM machine in experimental tests. It is also in expectation that there will be differences in the core losses even the amplitudes of phase currents are maintained the same.

In addition to the higher torque capability, the 6-phase configuration provides some redundancy for the windings and converters, and thus better fault tolerance. Three faulty conditions are mainly considered as an example, i.e., one phase lost (Faulty 1), two phase lost (PhA and PhB, Faulty 2), and 3 phase lost (PhA, PhB and PhC, Faulty 3), in comparison with the healthy condition. Torque waveforms, average torque and torque ripple are shown in Fig. 5a and Fig. 5b. These two figures illustrate the torque performance of the machine itself without considering special fault-tolerant control to reduce the torque ripple. Disturbance-free post-fault control strategies without introducing additional torque ripples by optimizing the currents of active phases can be used, as exemplified in [7] and [8], to protect the attached power converters and controllers from being damaged by mechanical vibration.

Considering the torque/power capability and fault tolerance, the 6-phase winding configuration has been selected and used in the design and prototyping of the proposed IMMD.

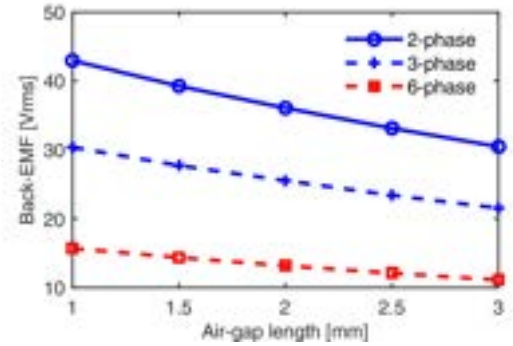

(a)

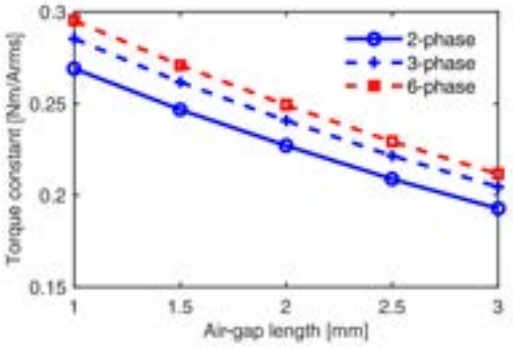

(b)

Fig. 4: Influence of air-gap length of the AFPM machine in the proposed IMMD on: (a) open-circuit phase back-EMF, (b) torque constant.

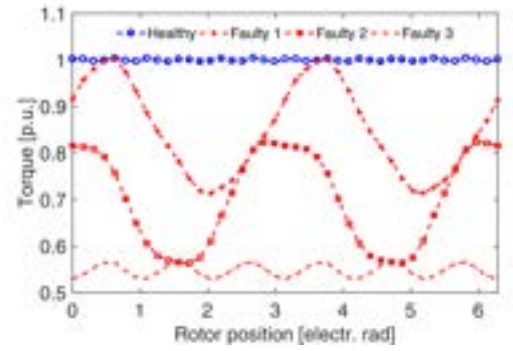

(a)

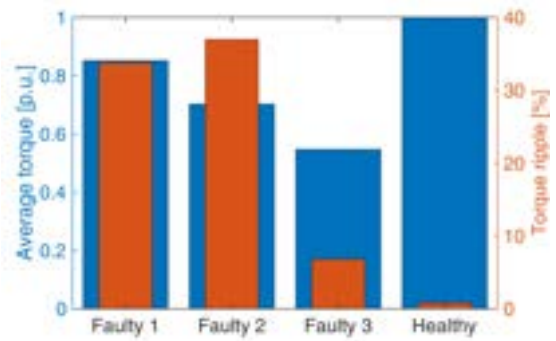

(b)

Fig. 5: Comparison of torque performance under healthy and various faulty conditions of the 6-phase configuration: (a) torque waveforms, (b) average torque and torque ripple.

IV. Evaluation of Further Torque Improvement

The 3rd harmonic in the MMF created by rotor PMs can be made full use of to enhance the electromagnetic torque by injecting 3rd current harmonics into the sinusoidal winding excitations and synchronizing multiple rotating magnetic fields, as discussed in [9], [10]. The underlying principle has been illustrated in Fig. 6.

With the pure sinusoidal current excitation, the stator MMF created by stator windings $f_s(\phi, t)$ has a sinusoidal component that leads the fundamental of the rotor MMF by 90deg. The interaction between these two fundamental MMFs produces the average torque. The rotor MMF and stator MMF created by currents with 3rd harmonic current injected (Fig. 7), are plotted in Fig. 8. When the 3rd harmonic currents are injected, the phase currents will take the forms of:

$$i_A = I_1 \sin(\omega t + \gamma) + I_3 \sin\left[3(\omega t + \gamma)\right] \tag{1}$$

$$i_X = I_1 \sin(\omega t + \gamma - \frac{\pi}{6}) + I_3 \sin\left[3(\omega t + \gamma - \frac{\pi}{6})\right] \tag{2}$$

$$i_B = I_1 \sin(\omega t + \gamma - \frac{2\pi}{3}) + I_3 \sin\left[3(\omega t + \gamma - \frac{2\pi}{3})\right] \tag{3}$$

$$i_Y = I_1 \sin(\omega t + \gamma - \frac{2\pi}{3} - \frac{\pi}{6}) + I_3 \sin\left[3(\omega t + \gamma - \frac{2\pi}{3} - \frac{\pi}{6})\right] \tag{4}$$

$$i_C = I_1 \sin(\omega t + \gamma - \frac{4\pi}{3}) + I_3 \sin\left[3(\omega t + \gamma - \frac{4\pi}{3})\right] \tag{5}$$

$$i_Z = I_1 \sin(\omega t + \gamma - \frac{4\pi}{3} - \frac{\pi}{6}) + I_3 \sin\left[3(\omega t + \gamma - \frac{4\pi}{3} - \frac{\pi}{6})\right] \tag{6}$$

where i_A, i_X, i_B, i_Y, i_C, and i_Z are the current excitations for the six phases. I_1 and I_3 are the amplitudes of the fundamental and 3rd harmonic current components. ω is the electrical angular frequency, t the time, and γ the initial phase angle.

It can be seen that, the resultant stator MMF to make full use of the 3rd harmonic of the square-wave rotor MMF approaches a triangular shape. This can also be observed from the analytical equations for rotor and stator MMFs shown in (7) and (8).

$$f_r(\phi, t) = \frac{4}{\pi} F_{PM} \sum_{k=1,3,5,\ldots}^{\infty} \frac{1}{k} \sin\left[k\left(5\phi - \omega t\right)\right], \tag{7}$$

$$\begin{aligned} f_s(\phi, t) =& A_{5,1} N_t I_1 \sin\left(5\phi - \omega t - \gamma + \frac{\pi}{2}\right) \\ & - A_{15,3} N_t I_3 \sin\left\{\left[3\left(5\phi - \omega t - \gamma + \frac{\pi}{2}\right)\right]\right\} \\ & + R_{em}, \end{aligned} \tag{8}$$

where $A_{5,1}$ and $A_{15,3}$ are the amplitudes of the 10-pole MMF created by the fundamental current and the 30-pole MMF (3rd harmonic) created by the 3rd harmonic current in the stator windings. Their values are $A_{5,1} = \frac{1}{2\pi}\frac{12}{5}\sqrt{2+\sqrt{3}}$ and

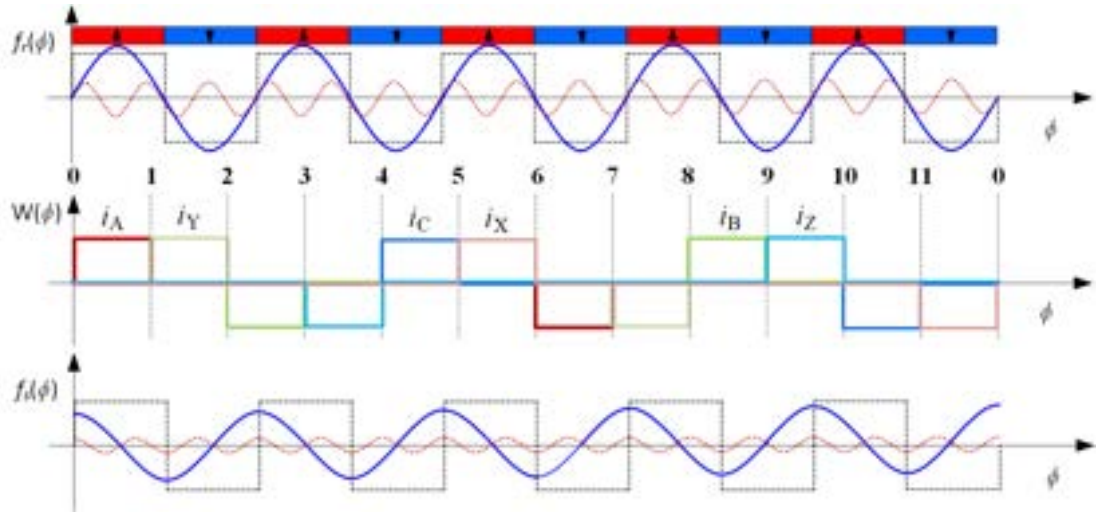

Fig. 6: MMF analysis of the 12s10p machine.

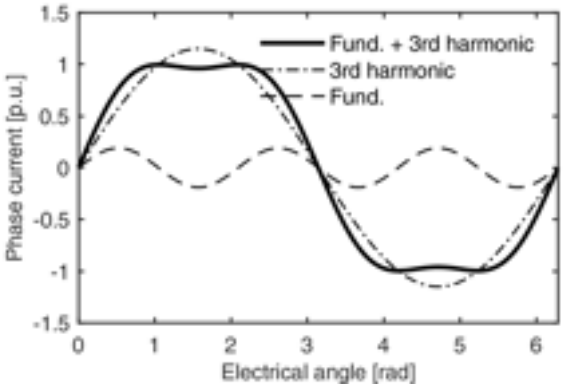

Fig. 7: Current waveform with 3rd harmonic current injection.

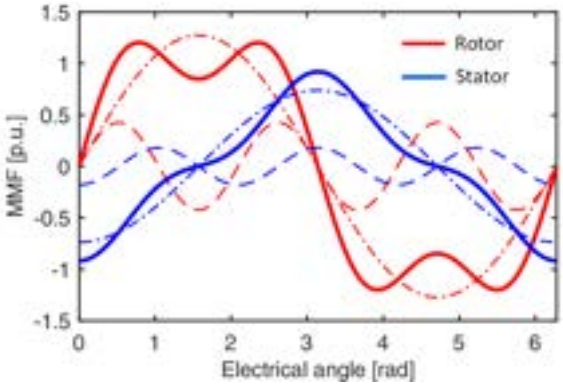

Fig. 8: Rotor and stator MMFs with 3rd current harmonic

$A_{15,3} = \frac{1}{2\pi}\frac{12}{5}\frac{1}{3}\sqrt{2}$, respectively. I_1 and I_3 are the amplitudes of the fundamental and 3rd harmonic current components. ϕ is the mechanical angle along the air-gap peripheral, ω the electrical angular frequency, t the time, and γ the phase angle, R_{em} the remainder term.

Ideally, the radially magnetized PMs in radial-flux PM machines will create a square wave MMF and the amplitude of the 3rd harmonic, will be 1/3 of the fundamental one. In real 12s10p machines with surface-mounted rotor PMs, the 3rd field harmonic, whose number of pole pairs is 15, is about 20% of the fundamental even with a very small physical air gap and semi-closed slot profiles. Large slot openings commonly used in 12s10p AFPM machines will increase the content of the 3rd field harmonic despite the fundamental will be reduced, as shown in Fig. 9a and Fig. 9b. In addition, the 12 stator teeth introduce the air-gap magnetic field modulation effect [11], which increases the amplitudes of sideband field harmonics of $(12-5)$ and $(12+5)$ pole pairs.

The increase in the 3rd field harmonic introduced by the large slot openings seems beneficial to the torque production, whereas further studies show that the contribution of the 3rd harmonic to the open-circuit back-EMF of the 12s10p AFPM machine is marginal due to the relatively large air-gap length (1.5mm - 3.0mm). As a result, the of torque enhancement by injecting the 3rd current harmonic and utilizing the 3rd field harmonic in the rotor MMF, as illustrated in Fig. 8, is ineffective for the 12s10p AFPM machine under study. The torque increase will only be contributed by the increased fundamental current when the 3rd harmonic current is injected, as shown in Fig. 7, given the same peak or rms value of the phase current. The torque improvement by this contributing factor is approx. 15% when the phase current peak value is kept the same.

V. Proof-of-concept Design

The AFPM machine in the lab used to build an IMMD is shown in Fig. 10, which has been evaluated in [12] as a 3-phase motor. The specifications are tabulated in TABLE I.

The stator core with full open slots was made of soft magnetic composites. Twelve concentrated coils were wound on plastic bobbins and then put on to stator teeth. The green printed circuit board (PCB) underneath the stator core in Fig. 10a was used for coil connections and will be replaced by the converter modules illustrated in Fig. 2. The rotor PMs are ferrite bonded to form a ring and magnetized in the axial

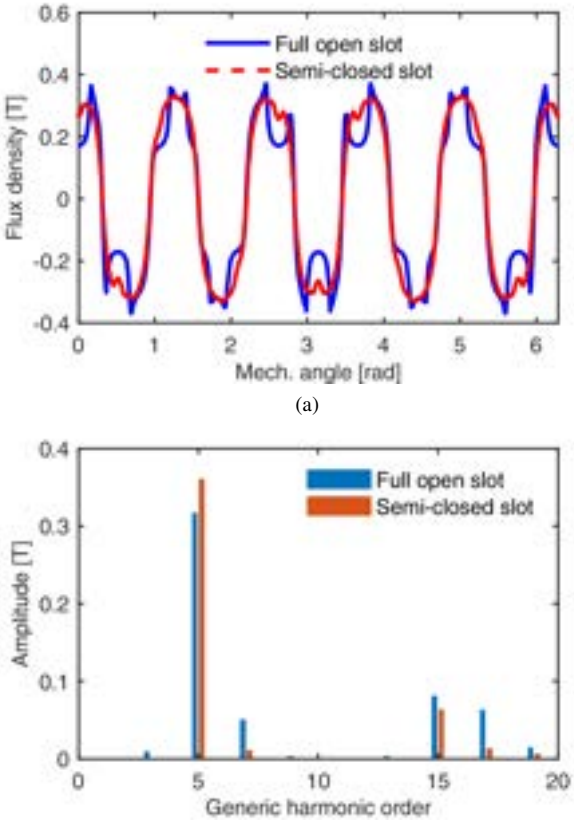

Fig. 9: Air-gap flux density at the mean diameter of the AFPM machine from 3D FEA: (a) waveforms, (b) amplitude spectrums. "Semi-closed slot" refers to the model whose tooth tops were widened and a fixed slot opening width was used.

TABLE I: Ratings and Specifications of the AFPM Machine

Rated torque [Nm]	1.12
DC bus voltage [V]	60
Rated current [Arms]	4.4
Outer/inner diameter [mm]	100/65
Stator/rotor axial length [mm]	34.0/12.4
Air-gap length [mm]	1.0-3.0 (adjustable)

direction. The measured open-circuit back-EMFs shown in Fig. 11 and Fig. 12 indicate good balance between phases.

VI. Conclusion

This paper presents a solution to use common AFPM machines with fractional-slot concentrated windings in IMMDs to reduce the overall volume and mass of the motor and its associated drive system based on a systematic comparison of different winding configuration possibilities.

Though all the winding configurations can be used to build the IMMD, the 2-phase configuration has the unique feature of electromagnetically isolated phases leading to high fault tolerance as a generator, and is suitable for low-cost motor drive with a single-phase input using as few as 6 switches. The 3-phase winding configuration shows an advantage by using the standard 3-phase converters. By contrast, the 6-phase

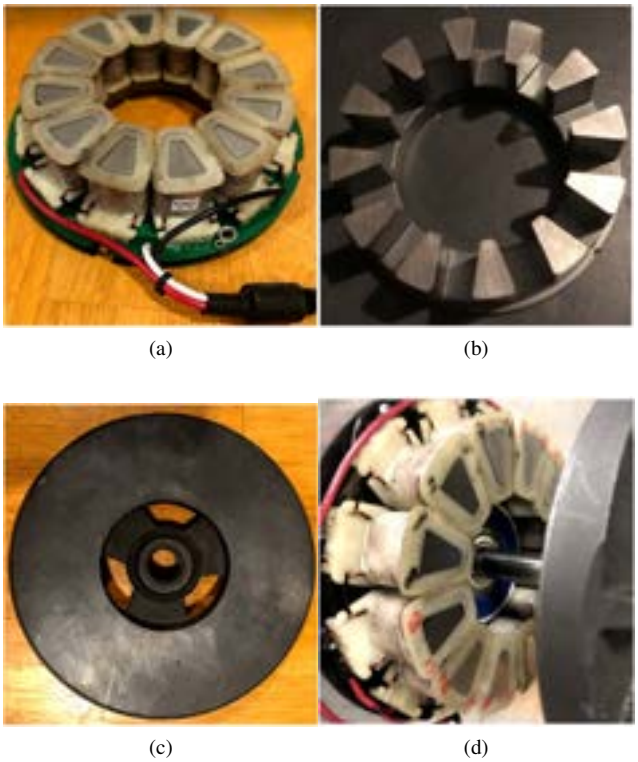

Fig. 10: The 12s10p AFPM machine under study, (a) stator with concentrated coils, (b) stator core with full open slot, (c) rotor with bonded ring magnets, (d) stator mounted to the test fixture.

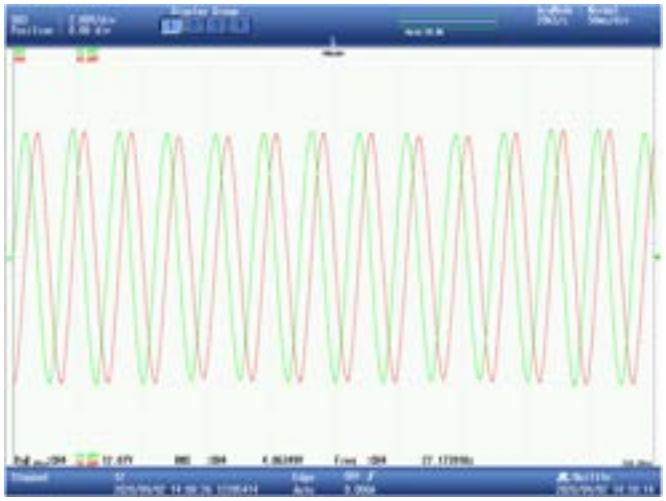

Fig. 11: Measured open-circuit back-EMF at 544r/min for the 2-phase winding configuration. The air-gap length was set to 2.7mm.

winding configuration provides better torque/power capability and fault tolerance for the same phase current rating and dc bus voltage.

An approx. 15% further torque enhancement is possible for the 6-phase configuration by injecting 3rd harmonic current when maintaining the same phase current peak value. The 3rd field harmonic in the rotor MMF created by axially magnetized PMs in AFPM machines cannot be utilized any more due to the relatively large physical air gap and full open slot profiles.

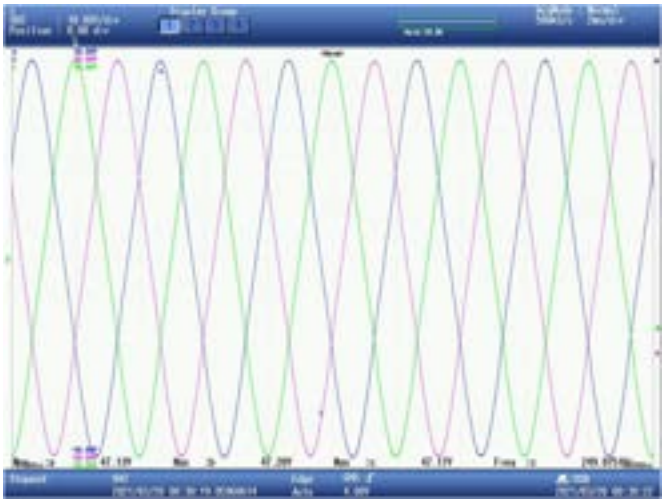

Fig. 12: Measured open-circuit back-EMF at 3,000r/min for the 3-phase winding configuration. The air-gap length was set to 1.5mm.

A 12s10p AFPM motor available in the lab is used to build the 6-phase IMMD for experimental validations.

ACKNOWLEDGMENT

The support of Regal Beloit Corporation, University of Kentucky, the L. Stanley Pigman Endowment, and Ansys, Inc., is greatfully acknowledged.

REFERENCES

[1] T. M. Jahns and B. Sarlioglu, "The incredible shrinking motor drive: Accelerating the transition to integrated motor drives," *IEEE Power Electron. Mag.*, vol. 7, no. 3, pp. 18–27, 2020.

[2] W. Lee, S. Li, D. Han, B. Sarlioglu, T. A. Minav, and M. Pietola, "A review of integrated motor drive and wide-bandgap power electronics for high-performance electro-hydrostatic actuators," *IEEE Trans. Transport. Electrif.*, vol. 4, no. 3, pp. 684–693, 2018.

[3] N. R. Brown, T. M. Jahns, and R. D. Lorenz, "Power converter design for an integrated modular motor drive," in *in Rec. IEEE Ind. Appl. Annu. Meeting*, 2007, pp. 1322–1328.

[4] J. Wang, Y. Li, and Y. Han, "Integrated modular motor drive design with GaN power FETs," *IEEE Trans. Ind. Appl.*, vol. 51, no. 4, pp. 3198–3207, 2015.

[5] S. Wu, C. Tian, W. Zhao, J. Zhou, and X. Zhang, "Design and analysis of an integrated modular motor drive for more electric aircraft," *IEEE Trans. Transport. Electrif.*, vol. 6, no. 4, pp. 1412–1420, 2020.

[6] V. Rallabandi, P. Han, M. G. Kesgin, N. Taran, and D. M. Ionel, "Axial-field vernier-type flux modulation machines for low-speed direct-drive applications," in *Proc. IEEE Energy Convers. Congr. Expo. (ECCE)*, 2019, pp. 3123–3128.

[7] R. Kianinezhad, B. Nahid-Mobarakeh, L. Baghli, F. Betin, and G. A. Capolino, "Torque ripples suppression for six-phase induction motors under open phase faults," in *Proc. Annu. Conf. IEEE Ind. Electron. (IECON)*, 2006, pp. 1363–1368.

[8] W. N. W. A. Munim, M. J. Duran, H. S. Che, M. Bermúdez, I. González-Prieto, and N. A. Rahim, "A unified analysis of the fault tolerance capability in six-phase induction motor drives," *IEEE Transactions on Power Electronics*, vol. 32, no. 10, pp. 7824–7836, 2017.

[9] A. Banerjee, J. H. Lang, and J. L. Kirtley, "Fine grain commutation: Integrated design of permanent-magnet synchronous machine drives with highest torque density," in *Proc. Int. Conf. Electr. Mach.*, 2012, pp. 671–677.

[10] K. Wang, Z. Q. Zhu, Y. Ren, and G. Ombach, "Torque improvement of dual three-phase permanent-magnet machine with third-harmonic current injection," *IEEE Trans. Ind. Electron.*, vol. 62, no. 11, pp. 6833–6844, 2015.

[11] M. Cheng, P. Han, and W. Hua, "General airgap field modulation theory for electrical machines," *IEEE Trans. Ind. Electron.*, vol. 64, no. 8, pp. 6063–6074, 2017.

[12] N. Taran, G. Heins, V. Rallabandi, D. Patterson, and D. M. Ionel, "Evaluating the effects of electric and magnetic loading on the performance of single- and double-rotor axial-flux pm machines," *IEEE Trans. Ind. Appl.*, vol. 56, no. 4, pp. 3488–3497, 2020.